A semiclassical study of wave packet dynamics in anharmonic potentials

Shilong Yang, Jianshu Cao,[a] and Robert W. Field[b]
Department of Chemistry, Massachusetts Institute of Technology Cambridge, Massachusetts 02139

(Received 21 April 2004; accepted 19 July 2004)

Classical and semiclassical methods are developed to calculate and invert the wave packet motion measured in pump-probe experiments. With classical propagation of the Wigner distribution of the initial wave packet created by the pump pulse, we predict the approximate probe signal with slightly displaced recurrence peaks, and derive a set of first-order canonical perturbation expressions to relate the temporal features of the signal to the characteristics of the potential surface. A reduced dynamics scheme based on the Gaussian assumption leads to the correct center of mass motion but does not describe the evolution of the shape of the wave packet accurately. To incorporate the quantum interference into classical trajectories, we propose a final-value representation semiclassical method, specifically designed for the purpose of computing pump-probe signals, and demonstrate its efficiency and accuracy with a Morse oscillator and two kinetically coupled Morse oscillators. For the case of one-color pump probe, a simple phase-space quantization scheme is devised to reproduce the temporal profile at the left-turning point without actual wave packet propagation, revealing a quantum mechanical perspective of the nearly classical pump-probe signal.
 [DOI: 10.1063/1.1791131]

I. INTRODUCTION

Recent advances in ultrafast laser spectroscopy offer a great opportunity to study elementary chemical processes at the molecular level. With femtosecond laser pulses it is now possible to create a coherent superposition of several vibrational states. Among many femtochemistry techniques, the pump-probe method is a key scheme to monitor molecular dynamics.[1–14] An ultrashort pump pulse promotes the ground state wave function onto the excited state at an *a priori* known position. Another ultrashort probe pulse at a later time measures the population at the probe position.[10] In ideal cases, the initial wave packet is an exact replica of the ground state wave function, and the width is fully determined by the ground state potential for a short pump pulse. Similarly, the internuclear distance sampled by the probe is selected by the wavelength of the probe pulse. A typical example we consider here is a molecule in the vibrational ground state of its electronic ground state. With an extremely short pulse, the ground state wave function is transferred to the excited state as a wave packet, which is a superposition of the vibrational states of the excited electronic state. As the center of wave packet oscillates between the inner and outer turning points on the excited state potential, the wave packet periodically spreads out and refocuses. However, such refocusing is not perfect due to the anharmonicity of the potential. As a superposition of a discrete set of vibrational states with different frequencies, the wave packet experiences partial revivals as the components of the wave packet dephase. Such dephasing and partial refocusing are vivid manifestations of the anharmonicity and provide extremely useful information about the general properties of the potential. Further progress in pulse shaping and coherence control opens a unique frontier for manipulating molecules on extremely short time scales, and provides an elegant way to control the dynamics of the wave packet. Therefore, it is crucial to develop a quantitative understanding of the causal relationship between specific features of the wave packet dynamics and the general features of the excited state potential.

There have been extensive studies of wave packet dynamics, including Gaussian wave packet dynamics, extended Gaussian wave packet dynamics in complex phase space, semiclassical coherent state methods, cellular dynamics methods, etc.[15–19] These studies have greatly enhanced the efficiency and accuracy of numerical calculations of wave-packet dynamics in many different potentials, yet an analytical relationship between the dynamics and the anharmonicity is still not available. In this paper, we will derive analytical expressions for the general features of the time domain signal, which are quantitatively related to the parameters of the potential. The motivation of this paper and related studies is to provide a potential inversion scheme for the excited state potential with a simple time domain measurement of wave-packet dynamics. Specifically, we study the Morse potential in this paper. The recurrences in the time domain dynamics are fully analyzed with canonical perturbation analysis, giving analytical relations to the Morse parameters: the fundamental frequency ω_0, the anharmonicity β, and the internuclear distance q_0. The quantitative expressions from the classical perturbation are employed to numerically invert the time domain signal, yielding first-order estimates of the Morse parameters.

To simulate the pump-probe signals, a full quantum calculation is usually expensive and practically impossible for large systems. Often, the full quantum calculation is accurate but gives little information about the underlying physics of the wave packet dynamics, such as the breakup and the par-

[a]Electronic mail: jianshu@mit.edu
[b]Electronic mail: rwfield@mit.edu

tial revival of the wave packet. On the other hand, the semiclassical method starts from the classical paths and their interferences to build up the complex amplitude, yielding detailed trajectory information about the underlying quantum dynamics. In this paper we adopt a revised version of the semiclassical initial-value representation (IVR),[20] and take advantage of the fixed probe position in pump-probe experiments. In our approach, we switch from the initial-value representation to the final-value representation, thus reducing the integration to the final momentum only. This semiclassical final-value representation is specifically designed to calculate pump-probe signals and has great potential advantages in multidimensional systems. When both pump and probe pulses are tuned to the left-turning point, we can further approximate the semiclassical final-value representation with a simple phase-space quantization scheme, which yields accurate information exclusively for the recurrences at the left turning point. This phase-space quantization scheme is inspired by discussions of linear and nonlinear response functions in anharmonic potentials addressed by Wu and Cao in Ref. 21, where phase-space quantization and averaging is employed to establish the classical-quantum correspondence of linear and nonlinear response functions.

The paper is organized as follows: In Sec. II, we discuss the classical wave packet dynamics in a Morse potential and derive quantitative relations between the wave packet revivals and the parameters of the potential with canonical perturbation analysis. In Sec. III, the semiclassical final-value representation is used to calculate the pump-probe signal, and compared with the exact quantum propagation. In Sec. IV, we propose a simple quantization scheme to evaluate the pump-probe signal at the left-turning point. As an example of a multidimensional case, we apply the semiclassical methods to two kinetically coupled Morse oscillators in Sec. V.

II. CLASSICAL WAVE-PACKET DYNAMICS

For simplicity, we consider a wave packet residing on the excited electronic state potential. The initial wave function is a perfect replica of the ground state wave function and is assumed to be in Gaussian form,

$$\Psi(q)=(2\pi w_0^2)^{-1/4}\exp\left[-\frac{(q-q_0)^2}{4w_0^2}\right], \tag{1}$$

where q_0 is the displacement between the excitation position and minimum of the excited state potential, and w_0 is the width of the wave packet. To proceed, we perform a Wigner transform and calculate the distribution function in phase space,

$$\begin{aligned}\rho_w(q,p)&=\frac{1}{2\pi\hbar}\int d\,\delta q\Psi^*\left(q+\frac{\delta q}{2}\right)\\&\quad\times\exp\left[\frac{i}{\hbar}p\,\delta q\right]\Psi\left(q-\frac{\delta q}{2}\right)\\&=\frac{1}{\pi\hbar}\exp\left[-\frac{(q-q_0)^2}{2w_0^2}-\frac{2w_0^2p^2}{\hbar^2}\right],\end{aligned} \tag{2}$$

which satisfies the minimum uncertainty condition $\sqrt{\langle\delta q^2\rangle\langle\delta p^2\rangle}=\hbar/2$. The wave packet then evolves on the excited state potential energy surface.

Classically, each particle moves on the potential surface following Newton's equations of motion. For a Morse potential, we can take advantage of the well-known action-angle variables, and express the position and momentum analytically as

$$\begin{aligned}q&=\frac{1}{\beta}\ln\frac{1-\sqrt{1-\lambda^2}\cos\phi}{\lambda^2},\\p&=\frac{\mu\omega_0\lambda}{\beta}\frac{\sqrt{1-\lambda^2}\sin\phi}{1-\sqrt{1-\lambda^2}\cos\phi},\end{aligned} \tag{3}$$

where λ is related to the action variable I as $\lambda=1-I/I_b$. The fundamental frequency ω_0 and the maximum action I_b for the Morse potential are $\omega_0=\sqrt{2D\beta^2/\mu}$ and $I_b=\sqrt{2D\mu/\beta^2}$, respectively. The Hamiltonian is given by

$$H=\frac{p^2}{2\mu}+D(1-e^{-\beta q})^2=\frac{\omega_0}{2}\left(2I-\frac{I^2}{I_b}\right), \tag{4}$$

and the time evolution of the angle variable is determined by $\dot{\phi}=\partial H/\partial I=\omega_0\lambda$. Through the action-angle variables, we define the transformation between the initial coordinates (q_i,p_i) and the final coordinates (q_t,p_t) at time t.

$$\begin{aligned}q_t(q_i,p_i)&=\frac{1}{\beta}\ln\frac{1-(1-\lambda^2e^{\beta q_i})\cos\omega_0\lambda t+(\mu\omega_0)^{-1}\beta p_i\lambda e^{\beta q_i}\sin\omega_0\lambda t}{\lambda^2},\\p_t(q_i,p_i)&=\frac{\mu\omega_0\lambda}{\beta}\frac{(\mu\omega_0)^{-1}\beta p_i\lambda e^{\beta q_i}\cos\omega_0\lambda t+(1-\lambda^2e^{\beta q_i})\sin\omega_0\lambda t}{1-(1-\lambda^2e^{\beta q_i})\cos\omega_0\lambda t+(\mu\omega_0)^{-1}\beta p_i\lambda e^{\beta q_i}\sin\omega_0\lambda t},\end{aligned} \tag{5}$$

where λ is an implicit function of q_i and p_i through the Hamiltonian in Eq. (4). The Jacobian of the transformation is proved to have a value of 1, which reflects conservation of phase-space volume. We can easily obtain the inverse transform $q_i(q_t,p_t)$ and $p_i(q_t,p_t)$ by reversing the roles of (q_i,p_i) and (q_t,p_t) in Eq. (5) and replacing t by $-t$. The classical orbits are sharp around the inner turning point where the repulsive potential is steep, and are flat around the outer turning point where the

attractive potential is shallow. The frequency of the orbit depends on the initial position due to anharmonicity; specifically, the orbits with higher energy have smaller frequency. As a result, the wave packet generally becomes spread out and twisted as it evolves.

To better illustrate the dephasing while the wave packet refocuses, we look into the probability distribution in phase space. Generally, the distribution at any time t can be written formally as

$$\rho_w(q,p,t)=\int\int \rho_w(q_i,p_i)\,\delta(q_t(q_i,p_i)-q) \times \delta(p_t(q_i,p_i)-p)\,dq_i dp_i, \tag{6}$$

where the two δ functions in the integration basically impose the dynamic constraint on the final coordinate in phase space. Applying the inverse transformation of Eq. (5), the phase-space distribution is given analytically as

$$\rho_w(q_t,p_t,t)=\rho_w[q_i(q_t,p_t),p_i(q_t,p_t)], \tag{7}$$

where the unity Jacobian is implicit. Initially the wave packet resides near $(q_0,0)$ in phase space. Hence the center of wave packet oscillates in the Morse potential with frequency $\omega_0\lambda_c$, where $\lambda_c=\sqrt{2e^{-\beta q_0}-e^{-2\beta q_0}}$ characterizes the center energy of the wave packet. However, other regions of the wave packet travel with different frequencies. Consequently, the wave packet cannot completely refocus; instead, it disperses in phase space. In Fig. 1, we show contour plots of the distribution $\rho_w(q_t,p_t)$ at the initial moment after excitation and at the center-of-packet period $t=2\pi/\omega_0\lambda_c$. The contours are obviously stretched and twisted due to the frequency mismatch, displaying rich phenomena in wave-packet dynamics.

Experimentally, the population monitored at the Franck-Condon excitation window is actually a specific integral form of the phase-space distribution $\rho_w(q_t,p_t,t)$, giving

$$N(q_0,t)=\int\int \rho_w(q_t,p_t,t)\,\delta(q_t-q_0)\,dq_t dp_t = \int \rho_w(q_0,p_t,t)\,dp_t. \tag{8}$$

For example, in the limit that the anharmonicity parameter β approaches zero while keeping ω_0 constant, the Morse potential in Eq. (4) reduces to the harmonic potential. Then, $N(q_0,t)$ reduces to

$$N(q_0,t)=\frac{1}{\sqrt{2\pi}w(t)}\exp\left[-\frac{[q_0-q_c(t)]^2}{2w^2(t)}\right], \tag{9}$$

where the center-of-packet motion $q_c(t)$ and the time dependent width $w(t)$ are given, respectively, by

$$q_c(t)=q_0\cos\omega_0 t, \qquad w^2(t)=w_0^2\cos^2\omega_0 t+\frac{\hbar^2}{4\mu^2\omega_0^2 w_0^2}\sin^2\omega_0 t. \tag{10}$$

Hence the width of the wave packet oscillates at twice the harmonic frequency ω_0, giving complete refocusing at both turning points. The deviation from complete refocusing is an explicit indication of the anharmonicity. To measure the anharmonicity, we examine the population signal in detail and obtain analytical expressions for the width of the initial decay, the recurrence time, and the recurrence amplitudes.

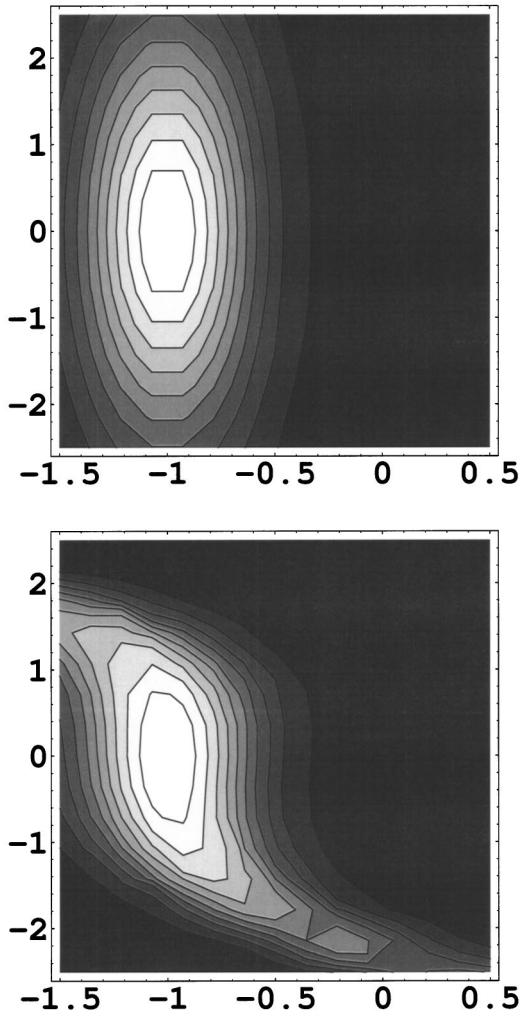

FIG. 1. The contour plots of the phase-space distribution at different times. The wave packet is initially created at the left-turning point $q_0=-1$ with width $w_0=1/\sqrt{12}$ and is propagated classically in the one-dimensional Morse potential with $D=30$ and $\beta=0.08$. The upper plot is the initial phase-space distribution, and the lower plot is the phase-space distribution at $t=2\pi/\omega_0\lambda_c$, where $\omega_0\lambda_c$ is the recurrence frequency for the center of the packet.

A. Dynamic features of the pump-probe signal and inversion

To calibrate the pump-probe signal, we calculate the width of the initial decay $\sigma_0^2=-M_0/M_2$ with $M_n=\partial_t^n|_{t=0}N(q_0,t)$. From the definition, we obtain the moments $M_0=(2\pi w_0^2)^{-1/2}$, $M_1=0$, and

$$M_2=(2\pi w_0^2)^{-1/2}[-\partial_q^2 V(q_0)-\hbar^2/(4\mu^2 w_0^4)] = (2\pi w_0^2)^{-1/2}[\omega_0^2(2e^{-2\beta q_0}-e^{-\beta q_0})-\hbar^2/(4\mu^2 w_0^4)],$$

where the first term is $-\partial_q^2 V(q_0)$, corresponding to the local curvature of the excited state potential at the center of wave packet. Here we consider the scenario that the initial excitation is a narrow wave packet so that the second term in M_2

always dominates, resulting in $M_2<0$. Thus the population decreases at early times, giving the width of the initial decay

$$\sigma_0^2=\left[\omega_0^2(e^{-\beta q_0}-2e^{-2\beta q_0})+\frac{\hbar^2}{4\mu^2 w_0^4}\right]^{-1}. \tag{11}$$

In order to investigate the anharmonic effects, we perform a canonical perturbation with respect to the anharmonic parameter $\beta=(\mu\omega_0/I_b)^{1/2}$. An important advantage of the canonical perturbation results is that the procedure can be generalized directly to other anharmonic potentials, for example, cubic or quartic oscillators. To proceed, we first study the frequency of the partial refocusing. The recurrence period of each classical trajectory is $\omega'=\omega_0\lambda$, with λ related to the initial position and momentum by Eq. (3). Expansion of ω' with respect to β yields the frequency for a given (q,p) configuration

$$\omega'\approx\omega_0\left[1-\frac{\beta^2}{2}\left(\frac{p^2}{\mu^2\omega_0^2}+q^2\right)\right]+O(\beta^3). \tag{12}$$

Due to the initial spreading in phase space, the recurrence frequency, as a function of (q,p), is no longer constant for all trajectories. Instead, ω' has a distribution around its average,

$$\begin{aligned}\langle\omega'\rangle&\approx\omega_0\left(1-\frac{\beta^2}{2}q_0^2\right)-\omega_0\frac{\beta^2}{2}\left[\frac{\langle\delta p^2\rangle}{\mu^2\omega_0^2}+\langle\delta q^2\rangle\right]\\&=\omega_0\left(1-\frac{\beta^2}{2}q_0^2\right)-\omega_0\frac{\beta^2}{2}\left[\frac{\hbar^2}{4\mu^2\omega_0^2 w_0^2}+w_0^2\right],\end{aligned} \tag{13}$$

where the minimum uncertainty wave packet is applied in the final expression. The first term in ω' comes naturally from the center-of-packet motion while the second term is a manifestation of the initial wave packet width. From the expression, an upper bound for the frequency can be obtained using the Cauchy inequality, $\langle\omega'\rangle\leqslant\omega_0(1-\beta^2q_0^2/2)-\beta^2\hbar/2\mu\leqslant\omega_0(1-\beta^2q_0^2/2)$. Hence, the mean recurrence time of the probe signal is

$$\begin{aligned}T=\frac{2\pi}{\langle\omega'\rangle}&\geqslant\frac{2\pi}{\omega_0(1-\beta^2q_0^2/2)-\beta^2\hbar/(2\mu)}\\&\geqslant\frac{2\pi}{\omega_0(1-\beta^2q_0^2/2)},\end{aligned} \tag{14}$$

indicating that the real recurrence time is always greater than the center-of-packet period, which is a consequence of the uncertainty principle.

Given the mean recurrence time, one can evaluate $N(q_0,t=T)$, with q_0 fixed at the Franck-Condon excitation position, yielding

$$\begin{aligned}\delta\omega'&=\omega'-\langle\omega'\rangle\\&=\omega_0\left[-\frac{\beta^2}{2}\left(\frac{p^2}{\mu^2\omega_0^2}-\frac{\hbar^2}{4\mu^2\omega_0^2 w_0^2}-w_0^2\right)\right]+O(\beta^3).\end{aligned} \tag{15}$$

In Eq. (15), we approximated $\cos\omega'T$ as 1 and $\sin\omega'T$ as $\delta\omega'T$, respectively. The inverse transform of Eq. (5) is estimated to second order in β as $q_i\approx q_0-p_t(\mu\omega_0)^{-1}\delta\omega'T$, $p_i\approx p_t+\mu\omega_0\delta\omega'T$, where $q_t=q_0$ at $t=T$ is applied implicitly. Consequently,

$$N(q_0,T)=\frac{\mu\omega_0}{\pi\hbar}\int_{-z_c}^{z_c}\exp[-h(z)]dz, \tag{16}$$

with the parameters z_c, z_0, and function $h(z)$, defined as

$$\begin{aligned}&z_c=\lambda_c/\beta\approx\beta^{-1}[1-\beta^2q_0^2/2],\quad z_0^2=\frac{\hbar^2}{4\mu^2\omega_0^2w_0^2}+w_0^2,\\&h(z)=\frac{\omega_0^2T^2\beta^4}{8}\left[w_0^{-2}z^2(z^2-z_0^2)^2+\left(\frac{\hbar}{2\mu\omega_0w_0}\right)^{-2}\right.\\&\qquad\left.\times q_0^2\left(z^2-z_0^2-\frac{2}{\beta q_0\omega_0T}\beta^{-1}z\right)^2\right].\end{aligned} \tag{17}$$

Combining Eqs. (11), (13), and (16), we derive quantitative relations between features of the time-domain pump-probe signals and the Morse parameters ω_0, β, and the internuclear distance q_0, thereby constructing a possible inversion scheme.

B. Numerical example: One-dimensional Morse potential

The canonical perturbation analysis of wave packet dynamics gives quantitative expressions for the width of the initial decay σ_0, the recurrence period T, as well as the first population recurrence $N(q_0,T)$. However, the classical phase-space propagation completely neglects quantum tunneling effects, hence it yields only a first-order estimate of the true quantum propagation. As an illustration, we evaluate the time domain pump-probe signal on the Morse potential using both quantum mechanics and classical mechanics. For the anharmonic potential, we use the same parameters, $D=30$ and $\beta=0.08$, as in Refs. 16, 17. The initial narrow Gaussian wave packet is created at the left turning point $q_0=-1$ with the width $w_0^2=1/12$. While the wave packet is oscillating between the left and right turning points, the excited state population $N(q_0,t)$ is probed at the left turning point as a function of time. In Fig. 2, $N(q_0,t)$ from both classical and quantum mechanical calculations are plotted. The dynamic features, σ_0, T, and $N(q_0,T)$, are calculated with Eqs. (11), (13), and (16) and compared with the quantum propagation in Table I. Clearly, the canonical perturbation analysis gives reasonable estimates of the width of the initial decay σ_0, the recurrence period T, and the first recurrence peak $N(q_0,T)$, but it is not able to provide quantitatively accurate information. In real experiments, population signals are collected at the probe position. To simulate the experiments, we use the temporal features calculated from quantum propagation to invert the Morse parameters ω_0, β, and the internuclear distance q_0. Here we adopt Powell's hybrid algorithm in the GNU Scientific Library and find the roots of the nonlinear equations (11), (13), and (16). The derivative matrix is evaluated using the finite difference method. The numerical results are summarized in Table I.

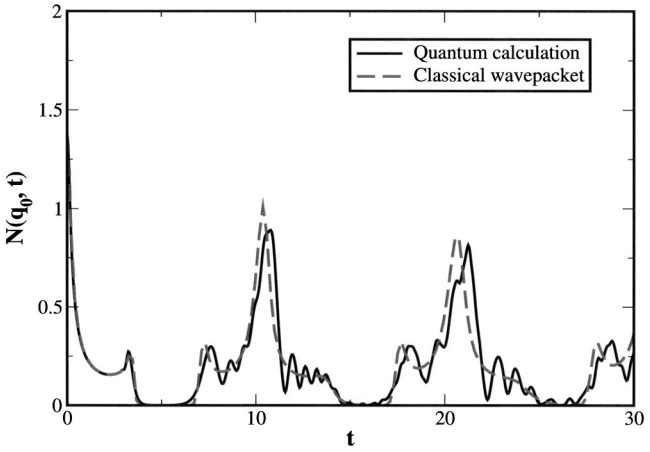

FIG. 2. Wave packet propagation on a one-dimensional potential with the same parameters given in Fig. 1 and Table I. The solid line is quantum propagation, and the dashed line is the classical propagation.

Although derived from a classical analysis, the calculation shows reasonable agreement with the exact parameters, giving a first-order inversion scheme.

C. Gaussian wave packet dynamics

The classical wave packet dynamics discussed in this section is obtained propagating the Wigner distribution that satisfies the minimum uncertainty condition. As an alternative, a reduced description is provided by the effective dynamics for the parameters of the wave packet instead of the evolution of the full distribution function. The best known example of this approach is Heller's Gaussian wave packet theory.[15,16] Interestingly, the one-dimensional Gaussian wave packet dynamics can be derived from the time-dependent variational method and is shown to be equivalent to the classical dynamics on an extended two-dimensional potential.[22,23] This version of Gaussian dynamics has stimulated recent studies[24] and will be adopted here for computing pump-probe signals. The difficulties of multidimensional extensions and the lack of convergence in the hierarchical construction preclude practical applications of this approach.

We introduce now the second-order cumulant expansion, and derive the equations of motion for the center and the width of the wave packet

$$\ddot{q}_c = -\langle \partial_q V \rangle_w , \tag{18}$$

$$\ddot{w} = -\langle \partial_q^2 V \rangle_w + \frac{\Delta}{w^3},$$

where $\langle \cdots \rangle_w$ represents the average over a Gaussian distribution centered at q_c with variance w^2, $\Delta = \hbar^2/4$ is a constant of motion under the second-order cumulant expansion, consistent with the minimum uncertainty condition. These coupled expressions indicate that the center and the width are both moving inside dressed potentials affected by wave-packet spreading. This Gaussian approximation becomes exact in the harmonic limit, recovering the results in Eq. (10). Once again, originating from the classical propagation of the Wigner distribution, the coupled Hamiltonian equation fails to capture the quantum interferences. This approach further assumes a Gaussian wave packet and introduces the second-order cumulant expansion, which allows us to propagate the parameters of the wave packet rather than the whole distribution. Although higher order cumulants can be included in the coupled Hamiltonian equations, an increase in the number of cumulants dramatically increases the complexity of the problem and does not provide a closed-form solution. Figure 3 shows that the coupled Hamiltonian equations can only reproduce the center-of-packet motion correctly but do not give an accurate description of the width-of-packet motion. Consequently, they cannot reproduce the population signal at the left-turning point. In comparison, the classical wave packet dynamics agrees quite well with the quantum solution for the center-of-packet motion, the width-of-packet motion, and the population signal.

In summary, Eq. (18) is equivalent to the second-order truncation of hierarchical Hamiltonian dynamics. Though inclusion of higher order moments improves the description of the shape of the wave packet, the numerical implementation is difficult for multidimensional systems. To incorporate quantum effects, we adopt a semiclassical method in the following section to calculate pump-probe signals with explicit interference effects.[20,25,26]

III. SEMICLASSICAL FINAL-VALUE REPRESENTATION

Classical wave packet propagation predicts the overall profile of the pump-probe signal but fails to reproduce the fine interference details. Obviously, classical propagation of a wave packet in phase space violates the uncertainty principle, and is fundamentally different from quantum mechanics. The pump-probe signal calculated with classical mechanics cannot fully reflect its intrinsically quantum nature. In

TABLE I. Comparison of the dynamic features of the pump-probe signal in the time domain. The initial wave packet is created at the left-turning point $q_0 = -1$ with $w_0^2 = 1/12$, and propagated in a one-dimensional Morse potential with $D = 30$ and $\beta = 0.08$. A numerical inversion of the quantum signal is performed with Eqs. (11), (13), and (16) obtained from classical phase-space propagation.

Dynamic features			Numerical inversion		
	Quantum	Classical		Exact	Estimate
T_1 (a.u.)	10.80	10.43	β (a.u.)	0.08	0.089
σ_0^{-2} (a.u.)	35.02	35.51	ω_0 (a.u.)	0.619	0.605
$N(q_0, T_1)$ (a.u.)	0.891	1.001	q_0 (a.u.)	−1.0	−1.08

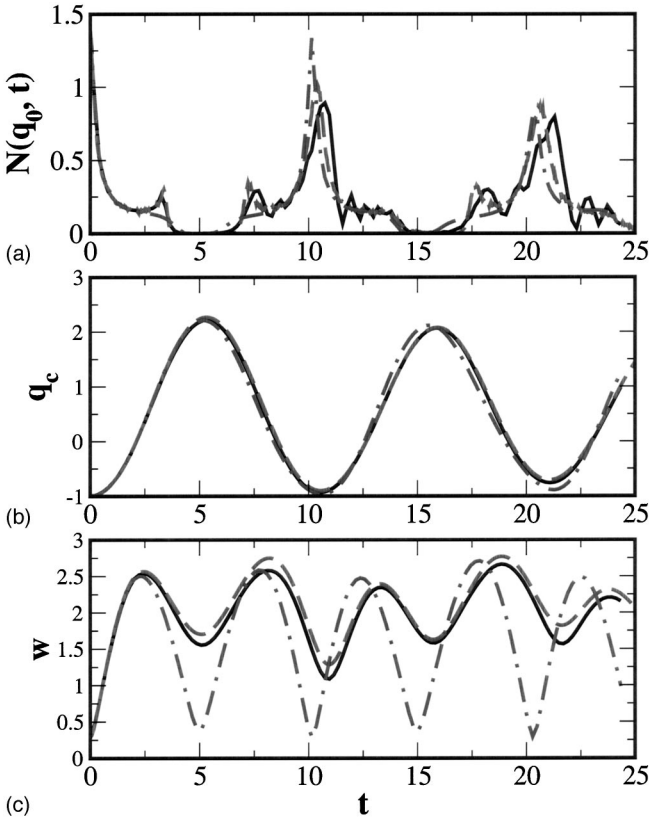

FIG. 3. (a) The population at the left-turning point, (b) the center of packet, and (c) the width of packet. Quantum results are plotted by solid lines, classical propagation results of the Wigner distribution are plotted by dashed lines, and the calculations of the coupled Hamilton dynamics are shown in dot-dashed lines. The parameters of the potential are the same as in Fig. 1.

general, the classical trajectories from different regions of the wave packet are not independent, but carry phase factors that interfere with each other. As a result, the pump-probe signal cannot be represented as a linear superposition of real populations, but a superposition of complex amplitudes. Formally, the pump-probe signal is well described by Feynman's path integral. To better illustrate the interference effects and calculate the pump-probe signal, we adopt a modified form of the IVR.[20] The initial-value phase-space integral representation has been discussed extensively by Miller and co-workers.[20,25,26] In the initial-value representation, the root trajectories that satisfy the two-point boundary conditions are replaced by an integration over the initial phase space area from which the classical trajectories evolve. The phase term in the initial-value representation is crucial for the trajectory interference.

Given an initial wave function in momentum space, the wave function at a later time t is formulated in coordinate space as

$$\Psi(q_t,t)=\langle q_t|e^{-iHt/\hbar}|\Psi(0)\rangle = \int dp_i \langle q_t|e^{-iHt/\hbar}|p_i\rangle \Psi(p_i,0), \tag{19}$$

where the propagator $\langle q_t|e^{-iHt/\hbar}|p_i\rangle$ is given[20] by

$$\langle q_t|e^{-iHt/\hbar}|p_i\rangle = \frac{1}{(2\pi i\hbar)^{N/2}} \sum_{q_i=q_i^{(k)}} \left|\det \frac{\partial q(t)}{\partial q_i}\right|^{-1/2} \times \exp\left\{\frac{i}{\hbar}[S(q_i,p_i,t)+q_i p_i] - i\frac{\pi}{2}\nu[q_i,t]\right\}. \tag{20}$$

The index $\nu[q_i,t]$ is the usual Maslov index for a trajectory crossing focal points and the summation is performed over the classical trajectories that satisfy the two-point boundary conditions. Obviously, the IVR expression involves both root searching and integration over the initial momentum in order to calculate the pump-probe signal for a given probe position q_t. So this approach is not numerically efficient and not applicable to high-dimensional systems. Furthermore, the Jacobian factor appears in the denominator of the semiclassical expression, causing a divergence at the caustics. Since classical mechanics has time-reversal symmetry, we can calculate the contributions from all classical trajectories by reverse propagating the classical trajectories from the final position q_t, yielding a "final-value representation," which is exactly analogous to the IVR. Rigorously, we change the integration variable from the initial momentum p_i to the final momentum p_t. By doing so, we introduce a Jacobian factor $|[\partial p_i/\partial p_t]_{q_t}|$, which is essentially the same as $|[\partial q(t)/\partial q_i]_{p_i}|$. The Maslov index remains the same. Consequently, we have the final-value representation expression for the wave packet propagation,

$$\Psi(q_t,t)=\int dp_t \left|\det\frac{\partial p_i}{\partial p_t}\right|^{1/2} (2\pi i\hbar)^{-N/2} \times \exp\left\{\frac{i}{\hbar}[S(q_t,p_t,t)+p_i q_i] + \frac{\pi}{2}\nu[p_t,t]\right\}\Psi(p_i,0), \tag{21}$$

where the initial position and momentum, q_i and p_i, are reverse propagations of q_t and p_t from time t. The extra Jacobian factor cancels the divergence at the caustics, thus making the integration numerically stable. For multidimensional cases, the integration over p_t can be done efficiently by a Monte Carlo scheme. The population monitored at the probe position is $N(q_t,t)=|\Psi(q_t,t)|^2$.

As a numerical example, Eq. (21) is calculated for several probe positions in the one-dimensional Morse potential. Probing at the left-turning point corresponds to the one-color pump-probe scheme where the probe pulse is tuned to the same wavelength as the pump pulse. Probing at the right turning point corresponds to a two-color pump-probe scheme where the probe pulse has a center frequency different from that of the pump pulse. The parameters of the potential as well as the initial wave packet are taken to be the same as in the preceding section. The results are compared with exact quantum calculations in Fig. 4. As shown in the plot, the final-value representation gives excellent agreement with the quantum results for both pump-probe schemes. All partial

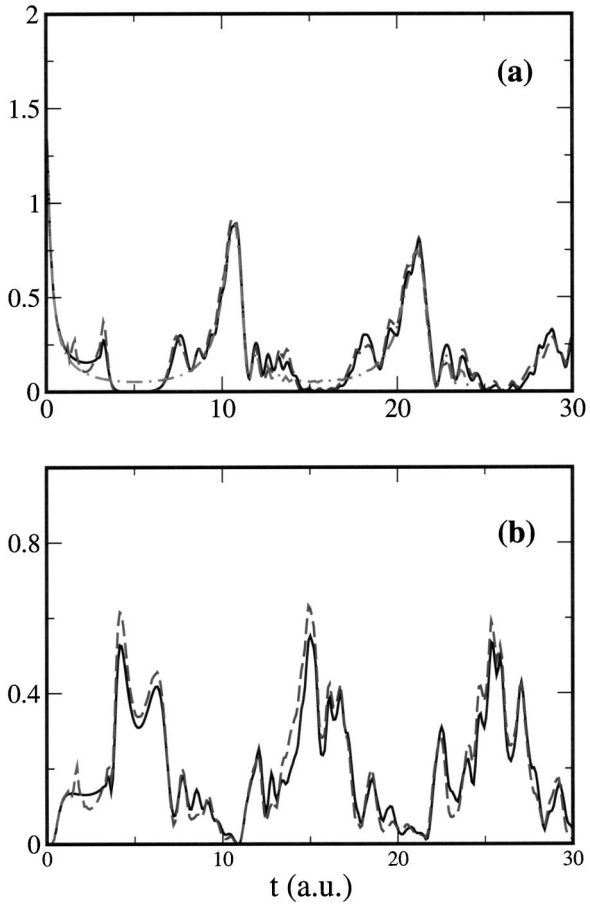

FIG. 4. The probe signals in a one-dimensional Morse potential are calculated using semi classical propagation and the quantum propagation (a) at the left-turning and (b) at the right-turning point. Quantum results are plotted in solid lines, the semiclassical results are plotted by dashed lines, and the results of the simple phase-space quantization approximation are plotted by dot-dashed line in (a). The parameters of the potential are the same as in Fig. 1.

revivals of the population and interference patterns are reproduced with excellent convergence. The small discrepancies between semiclassical calculations and the quantum calculations are due to the stationary phase approximation that underlies semiclassical dynamics.

IV. PHASE SPACE QUANTIZATION FOR THE LEFT-TURNING POINT SIGNAL

The final-value representation expression profits from the fixed probe position and the time-reversal symmetry of classical mechanics, providing an accurate and efficient way to calculate pump-probe signals. For pump-probe experiments where pump and probe positions are tuned to the same internuclear distance, we can further derive an approximation scheme from the semiclassical expression.

The integration over momentum space can be quantized as a summation over the discretized orbits which satisfy the Bohr or Einstein-Brillouin-Keller (EBK) quantization conditions. When the wave packet refocuses at the left turning point, the action term is approximately $2\pi\hbar(n+1/2)-E_n t$. The Jacobian factor is $|\partial p_i/\partial p_t|\sim 1$, giving the simple phase-space quantization expression

$$\Psi(q_t,t)\approx\sum_n \int_{V_n}(2\pi i\hbar)^{-1/2}\Psi(p_i,0)dp_i e^{ip_i q_t/\hbar}e^{-i\omega_n t}, \tag{22}$$

where V_n is the volume where the action variable satisfies $n\hbar\leqslant I<(n+1)\hbar$. It can be inferred from the above expression that the partial refocusing at the left turning point is mainly induced by anharmonic effects and the resultant dispersion in frequencies ω_n. From this point of view, the classical phase-space quantization scheme agrees with the quantum mechanical picture. The simple quantization scheme is a direct extension of phase space quantization and the averaging scheme of Ref. 21, where linear and nonlinear response functions are evaluated by a phase-space average around the quantized actions to establish the classical-quantum correspondence. Here we generalize this scheme to the evolution of the wave function at the left-turning point. This simple quantization scheme provides an easy way to estimate the signal at the left-turning point since the integration over V_n can be calculated straightforwardly given the quantization conditions. The coefficients then evolve with the eigenfrequency.

As shown in Fig. 4, numerical results demonstrate that the phase-space quantization method gives good approximations to the signals close to the revival periods, yielding correct peak positions as well as temporal widths. On the other hand, the approximation is compromised by the neglect of the Jacobian factor and crude estimation of the phase terms. Because it does not provide accurate information at probe positions other than the left-turning point, this approach cannot be applied to the two-color pump-probe scheme.

V. KINETICALLY COUPLED MORSE POTENTIAL

As an example of a well-characterized multidimensional problem, we apply the semiclassical final-value representation and the simple quantization scheme to the wave packet dynamics of two kinetically coupled Morse oscillators. Kinetically coupled Morse oscillators have been widely used to study the vibrational dynamics for *ABA* molecules, such as H_2O.[27–31] The generic Hamiltonian for these systems is

$$H=\sum_{j=1,2}\left[\frac{1}{2}G_{11}p_j^2+V(x_j)\right]+G_{12}p_1p_2, \tag{23}$$

where $V(x)=D[1-\exp(-\beta x)]^2$ is the Morse potential of a single O-H stretch, $G_{11}^{-1}=M_O M_H/(M_O+M_H)$ is the reduced mass for the O-H bond, and both bonds are dynamically coupled through the Wilson G-matrix element $G_{12}=\cos\theta_e/M_O$. θ_e is the angle between the two O-H bonds. In the absence of the coupling, the two Morse oscillators are independent, and thus the local mode description is exact. With the coupling, normal mode behavior dominates over a significant range of energy. However, due to anharmonic effects, there are many interesting dynamical features associated with the evolution from the normal mode to the local mode limit, which has been a central subject in vibrational spectroscopy. Extensive discussions of the normal to local mode transition can be found in papers by Brumer and co-workers.[27–29,31–33]

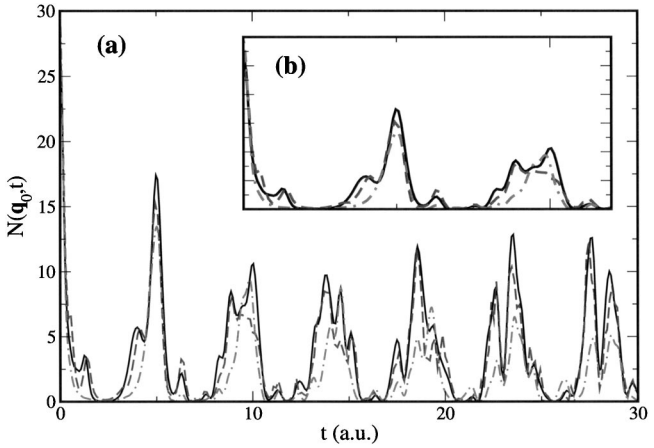

FIG. 5. Comparison of the phase-space quantization scheme, the semiclassical wave packet propagation, and the exact quantum calculation for two kinetically coupled Morse oscillators. The wave packet is initially created at $(-0.1,-0.1)$ with width $w_0=\sqrt{G_{11}\hbar/2\omega_0}/2$, and the parameters for H_2O are given in Table II. The probe signal is collected at the left-turning point. The quantum and semiclassical calculations are done with the full Hamiltonian in Eq. (23) while the phase-space quantization is done with the approximate Hamiltonian in Eq. (25). The inset (b) shows the first two recurrences. Quantum results are plotted by solid lines, the semiclassical results are plotted by dashed lines, and the results of the simple phase-space quantization approximation are plotted by dot-dashed lines.

To calculate the wave packet dynamics on the two-dimensional potential surface, we launch a Gaussian wave packet of the form $\Psi(\mathbf{q},0)=(2\pi w_0^2)^{-1/2}\exp[-(\mathbf{q}-\mathbf{q}_0)^2/(2w_0^2)]$ at the left-turning point and calculate the time-domain signal at another probe position $\mathbf{q}_t$. Although the semiclassical expression in Eq. (21) represents a considerable simplification of the original IVR formula, the integrand is an oscillatory function of the final momentum $\mathbf{p}_t$ and the integration in higher dimensions is generally a nontrivial calculation. Therefore one must introduce a positive definite weight function such that the Monte Carlo integration will be sampled only in those regions that dominate the integral. Other regions barely contribute to the integral due to phase cancellations. For example, the stationary phase Monte Carlo method has been widely applied to quantum mechanical path integral simulations. Since our main focus here is the semiclassical final-value representation, we simply apply a plain grid integration scheme to the two-dimensional case without invoking the stationary phase Monte Carlo method.

As a numerical example, the population at the left-turning point is calculated and plotted as a function of time in Fig. 5. The parameters are given in reduced units in Table II. Despite the small discrepancies, good agreement with the exact quantum results is achieved for a wide temporal range.

TABLE II. Parameters of H_2O.

	SI unit	Reduced unit
G_{11}	$6.353\times10^{26}\,\mathrm{kg}^{-1}$	1
G_{12}	$-9.427\times10^{24}\,\mathrm{kg}^{-1}$	-0.01484
$\hbar$	$1.0546\times10^{-34}\,\mathrm{kg\,m\,s}^{-2}$	1
D	$8.84\times10^{-17}\,\mathrm{J}$	1
β	$2.175\times10^{-10}\,\mathrm{n}^{-1}$	1

All of the partial revivals and decays, as well as detailed interference patterns, are accurately reproduced with excellent convergence. We believe the slight deviation from the quantum calculation is introduced by the underlying stationary phase approximation in the semiclassical approach. The final-value representation method, based on the IVR approach, is a promising candidate for calculations of the temporal trajectories of pump-probe signals. Furthermore, the semiclassical final-value representation contains all of the detailed information of classical trajectories and their interference effects, and is useful for studying the classical-quantum correspondence.

To test the accuracy of the simple quantization scheme in Sec. IV for the pump-probe signal at the left-turning point, we approximately quantize the phase space according to Sibert, Reinhardt, and Hynes. This approximate Hamiltonian is only necessary for the phase-space quantization scheme. In contrast, the full quantum calculation and the semiclassical propagation can be performed with the full Hamiltonian in Eq. (23). To proceed, we adopt a first-order approximation in the coupling term,[29,30] and write the full Hamiltonian in terms of the uncoupled action-angle variables, $H(I_1,I_2,\theta_1,\theta_2)=\Sigma_{i=1}^{2}(\omega_0 I_i-\omega_0^2 I_i^2/4D)+V(I_1,I_2,\theta_1,\theta_2)$. $V(I_1,I_2,\theta_1,\theta_2)$ is the coupling term for which exact Fourier analysis was performed by Jaffé and Brumer.[27] The leading order term is the 1-1 resonance term $V_{11}(I_1,I_2)\cos(\theta_1-\theta_2)$. When the Fourier coefficient V_{11} is approximately evaluated at the center of the resonance zone, one obtains

$$V_{11}\approx -V_0(E)=\frac{4D|G_{12}|}{G_{11}}\left(1-\frac{E}{2D}\right)\left|\frac{1-(1-E/2D)^{1/2}}{1+(1-E/2D)^{1/2}}\right|. \tag{24}$$

Performing the canonical transform, $I_1+I_2=P$, $\theta_1+\theta_2=2\phi$, and $I_1-I_2=p$, $\theta_1-\theta_2=2\psi$, the Hamiltonian can be approximated as

$$H\approx\omega_0 P-\frac{\omega_0^2P^2}{8D}-\frac{\omega_0^2p^2}{8D}-V_0(E)\cos 2\psi, \tag{25}$$

with $V_0(E)$ given in Eq. (24). The approximation breaks down outside the resonance zone where the 1-1 resonance term is no longer the dominant contribution to the dynamics. Bohr quantization requires

$$\begin{aligned} I_\phi&=\frac{1}{2\pi}\int P\,d\phi=P=(n_\phi+1)\hbar,\\ I_\psi&=\frac{1}{2\pi}\int p\,d\psi\\ &\approx\frac{1}{2\pi}\int d\psi\sqrt{\frac{8D}{\omega_0^2}\left[\omega_0 P-\frac{\omega_0^2P^2}{8D}-E-V_0(E)\cos 2\psi\right]}\\ &=n_\psi\hbar, \end{aligned} \tag{26}$$

where n_ϕ and n_ψ are integers.

For a given pair of quantum numbers, the eigenenergy $E(n_\phi,n_\psi)$ is determined from the quantization requirements, hence the spectrum for the approximate Hamiltonian is fully resolved numerically. Given a phase-space point, the action-angle variables $(I_1,I_2,\theta_1,\theta_2)$, hence (P,p,ϕ,ψ), are well

defined. The approximate Hamiltonian in Eq. (25) provides a self-consistent way to solve for the energy E. With the energy term, the quantum numbers n_ϕ and n_ψ can be numerically determined with Eq. (26), giving the EBK quantized torus. Accordingly, we evaluate the phase-space quantization integrals used in the phase-space quantization scheme.

The pump-probe signal at the left-turning point is calculated and shown in Fig. 5. The quantum and semiclassical calculations are performed for the full Hamiltonian while the calculation with simple phase-space quantization is done for the approximate Hamiltonian in Eq. (25). Once again the phase-space quantization scheme correctly predicts the revivals as well as their widths, demonstrating reasonably good agreement with both quantum and semiclassical calculations. The shoulders on either side of the revival are mainly due to the Jacobian factor, which is reproduced by the simple quantization scheme.

VI. CONCLUDING REMARKS

To summarize, a quantitative analysis of the pump-probe signal in the Morse potential is performed with classical wave packet dynamics, relating the temporal features to characteristics of the potential surface. The quantitative relations, although derived completely from classical mechanics, provide a way to calculate the fundamental frequency ω_0, the anharmonicity β, and the initial internuclear distance q_0. An alternative classical wave packet method, coupled Hamiltonian dynamics, predicts the center-of-packet motion correctly but fails to give an accurate description of the width-of-packet motion. The interference effects neglected in classical wave packet propagation are incorporated using a semiclassical final-value representation (a variant of IVR), which is specifically designed to calculate pump-probe signals. Originating from the semiclassical initial-value representation, the final-value representation propagates classical trajectories by the reverse evolution of Newton's equations. In this way, the final-value representation reduces the initial phase-space integration to the final momentum and removes the divergences at the caustics, resulting in a numerically stable method that can be easily generalized to multidimensional systems. We demonstrate the efficiency and accuracy of the semiclassical final-value representation in examples of a one-dimensional Morse potential and two kinetically coupled Morse oscillators. In the case when the probe position coincides with the initial pump position, we make a further approximation at the left-turning point and derive a simple phase-space quantization scheme for the wave packet dynamics. In this approximation, the initial wave function is decomposed into segments according to phase-space quantization, and each segment evolves with the eigenfrequency of the corresponding orbit or torus. This simple quantization scheme gives excellent agreement at the left-turning point, predicting the correct recurrence time and revival width as well. Based solely on the approximation at the left-turning point, the simple quantization scheme does not provide accurate information at positions other than the left-turning point. Calculating wave packet dynamics with classical and semiclassical dynamics provides powerful tools to interpret experimental measurements and quantum mechanical calculations. Further efforts will be devoted to coupled oscillators and dissipative anharmonic systems.

ACKNOWLEDGMENTS

This research was supported by the NSF Career Award (Grant No. Che-0093210) and the Petroleum Research Fund administrated by the American Chemical Society. J.C. is a recipient of the Camille Dreyfus Teacher-Scholar Award. We are grateful to Professor Robert Silbey for stimulating discussions.

[1] D. J. Tannor, R. Kosloff, and S. A. Rice, J. Chem. Phys. **85**, 5805 (1986).
[2] S. A. Rice and M. Zhao, *Optical Control of Molecular Dynamics* (Wiley, New York, 2000).
[3] R. Bersohn and A. H. Zewail, Ber. Bunsenges. Phys. Chem. **92**, 373 (1988).
[4] R. E. Walkup, J. A. Misewich, J. H. Glownia, and P. P. Sorokin, Phys. Rev. Lett. **65**, 2366 (1990).
[5] B. Fain, S. H. Lin, and N. Hamer, J. Chem. Phys. **91**, 4485 (1989).
[6] Y. J. Yan, L. E. Friend, and S. Mukamel, J. Phys. Chem. **93**, 8149 (1989).
[7] W. T. Pollard, S.-Y. Lee, and R. A. Mathies, J. Chem. Phys. **92**, 4012 (1990).
[8] J. L. Krause, R. M. Whitnell, K. R. Wilson, and Y. J. Yan, in *Femtosecond Chemistry*, edited by J. Manz and L. Wöste (Springer-Verlag, Weinheim, 1995), p. 273.
[9] B. Kohler, J. L. Krause, F. Raksi, K. R. Wilson, R. M. Whitnell, V. V. Yakovlev, and Y. J. Yan, Acc. Chem. Res. **28**, 133 (1995).
[10] J. Cao and K. R. Wilson, J. Chem. Phys. **106**, 5062 (1997).
[11] J. Cao and K. R. Wilson, J. Chem. Phys. **107**, 1441 (1997).
[12] Y.-C. Shen and J. A. Cina, J. Chem. Phys. **110**, 9793 (1999).
[13] S. Garashchuk and D. J. Tannor, Annu. Rev. Phys. Chem. **51**, 553 (2000).
[14] C. Manescu, J. L. Krause, K. B. Møller, and N. E. Henriksen, J. Phys. Chem. A (to be published).
[15] E. J. Heller, J. Chem. Phys. **62**, 1544 (1975).
[16] E. J. Heller, J. Chem. Phys. **94**, 2723 (1991).
[17] F. Grossman, J. Chem. Phys. **103**, 3696 (1995).
[18] Y. Weissman, J. Chem. Phys. **76**, 4067 (1982).
[19] J. R. Klauder, Phys. Rev. Lett. **56**, 897 (1986).
[20] G. Campolieti and P. Brumer, Phys. Rev. A **50**, 997 (1994).
[21] J. Wu and J. Cao, J. Chem. Phys. **115**, 5381 (2001).
[22] F. Arickx, J. Broeckhove, E. Kesteloot, L. Lathouwers, and P. Van Leuven, Chem. Phys. Lett. **128**, 310 (1986).
[23] A. K. Pattanayak and W. C. Schieve, Phys. Rev. E **50**, 3601 (1994).
[24] O. V. Prezhdo and Y. V. Pereverzev, J. Chem. Phys. **116**, 4450 (2002).
[25] W. H. Miller, J. Chem. Phys. **53**, 1949 (1970).
[26] J. Cao and G. A. Voth, J. Chem. Phys. **104**, 273 (1996).
[27] C. Jaffé and P. Brumer, J. Chem. Phys. **73**, 5646 (1980).
[28] R. T. Lawton and M. S. Child, Mol. Phys. **37**, 1799 (1979).
[29] E. L. Sibert III, W. P. Reinhardt, and J. T. Hynes, J. Chem. Phys. **77**, 3583 (1982).
[30] E. L. Sibert III, J. T. Hynes, and W. P. Reinhardt, J. Chem. Phys. **77**, 3595 (1982).
[31] L. Xiao and M. E. Kellman, J. Chem. Phys. **90**, 6086 (1989).
[32] M. P. Jacobson, R. J. Silbey, and R. W. Field, J. Chem. Phys. **110**, 845 (1999).
[33] M. P. Jacobson, C. Jung, H. S. Taylor, and R. W. Field, J. Chem. Phys. **111**, 600 (1999).